2015

Atmospheric Responses to North Atlantic SST Anomalies in Idealized Experiments. Part I: Northern Hemispheric Circulation

Michael C. Veres
University of Nebraska-Lincoln, michael.veres@yahoo.com

Qi Hu
University of Nebraska - Lincoln, qhu2@unl.edu

Atmospheric Responses to North Atlantic SST Anomalies in Idealized Experiments. Part I: Northern Hemispheric Circulation

MICHAEL VERES AND QI HU

School of Natural Resources, and Department of Earth and Atmospheric Sciences, University of Nebraska–Lincoln, Lincoln, Nebraska

(Manuscript received 10 June 2014, in final form 30 April 2015)

ABSTRACT

Idealized model experiments using the NCAR CESM1.0.5 under equinox conditions are designed and performed to address two fundamental questions about the effects of the sea surface temperature (SST) variation associated with the Atlantic multidecadal oscillation (AMO) on circulation and precipitation in North America and Europe: 1) Is the observed relationship between the AMO SST and the warm-season precipitation in North America a statistical coincidence? and 2) Why is the response of negative precipitation anomaly to warm SST in the AMO fairly uniform across most of North America, whereas the positive precipitation anomaly in the cold SST rather spotty? Model experiments are done with either a warm or cold SST anomaly in an aquaplanet, a planet with idealized continents, and a planet with both idealized continents and orography. Major results show that the atmospheric response to warm SST anomaly in the North Atlantic is fairly similar among the three sets of experiments. In the lower troposphere, the response has a significant negative geopotential anomaly from the SST anomaly center to the east and a positive geopotential anomaly in upstream North America. However, the response to the cold SST anomaly changes considerably among these experiments, particularly in North America. These results provide a foundation to answer the abovementioned two questions. First, they show that there is physical connection of the AMO SST and atmospheric circulation anomalies in North America. Moreover, the rather stable atmospheric response to the warm SST may explain the observed largely consistent response to the warm SST anomaly. The varying responses of the atmosphere to the cold SST indicate a strong sensitivity of the atmosphere to other forcings during the cold SST anomaly in the North Atlantic. This sensitivity could explain the varying and less stable response of the atmosphere to the cold SST during the AMO.

1. Introduction

Summertime precipitation variations in the U.S. Great Plains are determined by numerous forcing factors and processes of both local and remote origin. Dependent on which forcings or processes are active at a particular season, year, or decade, they and their interactions could result in particular regional circulation anomalies that influence the region's precipitation in ways different from that influenced by a different set of forcings/processes. Such interactions among the forcings and associated processes complicate our efforts to understand and predict interannual, decadal, and longer time-scale variations in precipitation. To improve our understanding and prediction, we need to understand the individual forcings and their effects on the region's circulation and precipitation and, further, how their individual effects may change from interactions with other processes of different scales or origin.

In the Great Plains, several such forcings and associated processes have been identified. They include the low-level southerly jet (LLJ) from the Gulf of Mexico (e.g., Namias 1983; Mo et al. 1997; Higgins et al. 1997; Hu and Feng 2001b; Wang and Chen 2009), anomalous local surface fluxes of water and heat (e.g., Schubert et al. 2004), remote forcing from the sea surface temperature (SST) anomalies in the tropical Pacific Ocean [e.g., El Niño–Southern Oscillation (ENSO)] and the North Pacific Ocean [e.g., the Pacific decadal oscillation (PDO); e.g., Ting and Wang 1997; Hu and Feng 2001a], the Arctic Oscillation (Hu and Feng 2010), and the SST anomalies in the North Atlantic Ocean associated with the Atlantic multidecadal oscillation (AMO; e.g., Enfield et al. 2001; McCabe et al. 2004; Hu and Feng 2008).

Corresponding author address: Dr. Qi Hu, School of Natural Resources, and Department of Earth and Atmospheric Sciences, University of Nebraska-Lincoln, 707 Hardin Hall, 3310 Holdrege Street, Lincoln, NE 68583-0961.
E-mail: qhu2@unl.edu

DOI: 10.1175/JCLI-D-14-00413.1

Some effects of these individual forcings and their interactions on the U.S. Great Plains summertime precipitation have been examined in recent modeling and diagnostic studies (e.g., Wang et al. 2008; Hu et al. 2011; Hu and Feng 2012; Veres and Hu 2013). Among them, Hu et al. (2011) used the National Center for Atmospheric Research (NCAR) Community Atmosphere Model, version 3.1 (CAM3.1), and examined the AMO effects on the Great Plains summertime precipitation. They allowed AMO SST anomalies in the North Atlantic Ocean but specified climatological SST in the other oceans around the world and integrated the model for 20 years (and later extended to 100 years). Their analyses of the model results reveal different processes and effects of the warm and cold SST during the AMO on summertime circulation and precipitation in the Great Plains and throughout North America. In the midlatitude North America, their results show a fairly uniform sign of deficit precipitation (with varying magnitude) during the warm SST anomaly in the AMO (see Fig. 3 in Hu et al. 2011). In the cold SST anomaly, their results show positive precipitation anomalies but with a much varying pattern. The less consistent pattern of precipitation anomalies in response to the cold SST anomaly prompts the question of why the cold SST anomalies in the North Atlantic do not produce uniform or consistent surplus precipitation in the midlatitude North America as that forced during the warm SST anomaly in the AMO.

A quick answer to this question would be that different local and regional processes initiated and/or enhanced in the opposite phases of the AMO could have interfered with the AMO effect differently and resulted in different responses of circulation and precipitation in North America. Another possibility would be the nonlinearity of the atmospheric response to the different (warm vs cold) SST forcing of the AMO. While we are uncertain of any of these causes, it is certain that the model-simulated results in Hu et al. (2011) are not just the AMO effect. Those simulations show the collective outcome of the circulation and precipitation responses to the AMO and their modifications by some local, regional, and large-scale processes. In short, we still do not know yet what the *original* effects (i.e., unmodified by those processes) of the North Atlantic SST anomalies associated with the AMO are on North American summertime circulation and precipitation. We also do not know how this SST effect may have been changed by other prominent factors of the circulation system to yield the observed differences between the warm and cold phases of the AMO.

More results from previous studies also have alluded to the need to understand how these processes may interfere with one another and affect the atmospheric response to the AMO. Ringler and Cook (1999) surmise that variations in land surface conditions could alter the atmospheric response originally forced by the presence of that land surface. It is logical to extend that idea to question how the atmospheric response might interact with other remotely forced responses (i.e., the AMO). From this perspective, we can see a need to separate the direct atmospheric response to the AMO forcing and, then, to examine and understand how that response may be altered by, for example, land, land surface conditions, and orography.

In this study, we attempt to fill this need and answer the questions we raised earlier—that is, what are the original effects of the AMO on the atmospheric circulation, and why is the observed response to the cold SST in AMO so varying across North America? We will use a set of idealized model experiments. As the first step in this effort, we study the atmospheric responses at the equinox when excessive solar heating or longwave radiative cooling, as in the solstice, can be excluded in the model. Although the atmospheric response at the equinox could be different from that in boreal summer, the differences in the response to the warm and cold SST anomalies in the North Atlantic from the equinox experiments should shed light on the difference in atmospheric response to the opposite SST anomaly in the AMO in boreal summer.

We begin these experiments with an aquaplanet, and then extend to a planet with idealized continents without orography, and finally to a planet with idealized continents and orography. In each setting—for example, the aquaplanet—there will be three experimental runs. The first is the control run that uses zonally averaged climatological SST in all oceans. The second experiment has fixed warm SST anomalies in the latitude and longitude of the North Atlantic Ocean. The third experiment has cold SST anomalies fixed in the North Atlantic Ocean. The second and third runs represent the warm and cold phases of the AMO, respectively. The effects of the opposite SST anomalies on the atmospheric circulation will be evaluated from these model experiments. Results of the aquaplanet simulations will show the SST effects on atmospheric circulation and precipitation. Changes of such effects, which may be considered as the original AMO effect, caused by the presence of continents and orography can be identified from the differences between the aquaplanet results and the results from model runs with continents alone and continents plus orography. From these changes, we may find if and how such modifications may have contributed to the differences in atmospheric responses to the warm and cold SST forcing during the AMO.

TABLE 1. Summary of the experiments.

SST	Topography		Description
	Continents	Orography	
Control	No	No	Aquaplanet, zonally symmetric (control) SST
Cold	No	No	Aquaplanet, control SST with negative anomaly in the North Atlantic
Warm	No	No	Aquaplanet, control SST with positive anomaly in the North Atlantic
Control	Yes	No	Land, control SST
Cold	Yes	No	Land, control SST with negative anomaly in the North Atlantic
Warm	Yes	No	Land, control SST with positive anomaly in the North Atlantic
Control	Yes	Yes	Land and orography, control SST
Cold	Yes	Yes	Land and orography, control SST with negative anomaly in the North Atlantic
Warm	Yes	Yes	Land and orography, control SST with positive anomaly in the North Atlantic

To a certain extent, this approach is similar to that initially described by Inatsu et al. (2003) and later extended by Brayshaw et al. (2008, 2009, 2011) in their studies of the midlatitude storm tracks. In Inatsu et al. (2003), the atmospheric dynamics of the midlatitude storm tracks are examined in an idealized aquaplanet setting. The work of Brayshaw et al. extends that work from an aquaplanet to a planet with idealized continents and orography in order to gain understanding of the storm-track dynamics in a more realistic setting. In this study, we aim to expand upon some limitations in the study of Brayshaw et al. (2008, 2009). For example, the focus in Brayshaw et al. is on the direct effects of SST, land, and orography on the Northern Hemisphere storm track. The interactions among these direct effects are less focused upon. One interaction examined in their study is related to the SST anomaly in the North Atlantic Drift. In our study, we focus on the interactions of the SST anomalies resembling the AMO. In addition, we expand the orography experiments from that in Brayshaw et al. (2009, 2011) to include the Alps and the Tibetan Plateau, which according to prior studies (e.g., Ting 1994) can significantly improve simulations of the North American circulation. While the studies of Brayshaw et al. (2008, 2009, 2011) provide insight into how different forcings interact, the design of the current study allows for further understanding of the interactions and, hence, improve our comprehension of the North Atlantic SST effects on atmospheric circulation and precipitation in North America.

Details of the model and experimental design and justification for this study are described in the next section (section 2). Simulated global atmospheric circulations from the model experiments in an aquaplanet, a planet with continents and no orography, and a planet with continents and orography are examined and discussed in section 3. A summary of the results and the answers to our questions are given in section 4. It is important to note that the results presented in this article are the responses and some underline dynamic processes of Northern Hemisphere circulation to the AMO. Responses of North American precipitation and causal processes, such as storm-track and baroclinic instability, from these model experiments, as well as their comparisons with results from prior similar studies, are described in Hu and Veres (2014, manuscript submitted to *J. Climate*, hereafter Part II) of this two-part paper.

2. Model and experimental design

a. Model

We use the NCAR Community Earth System Model, version 1.0.5 (CESM1.0.5) in this study. The principle model components in CESM1.0.5 used in this study are the Community Atmosphere Model, version 5.1 (CAM5.1), and the Community Land Model, version 4 (CLM4). The horizontal resolution used is T85, equivalent to 1.4° in latitude and longitude. We use the CAM4 physics package, which has 26 vertical levels. The SST and its anomalies in the model are prescribed using analytical functions, and sea ice is prevented from forming.

b. Experiment details

Table 1 summarizes the nine experiments designed and performed in this study. All these experiments were run under perpetual equinox conditions. Under such conditions, we prevent excessive cooling or warming as in the winter or summer hemisphere due to minimal or maximal solar insolation. Thus, the model can reach equilibrium, and a steady-state solution is reached in each run. Each run is for 20 years. It reaches equilibrium within a few months after the start because the SST is prescribed.[1] To be cautious, we discard the first 2 years of the simulation as spinup and use the data from years 3 to 20 in our analysis.

[1] Temporal variations in surface energy fluxes in all the experiments were examined and were found fluctuating at a constant value. Thus, no drift occurs in the model simulations.

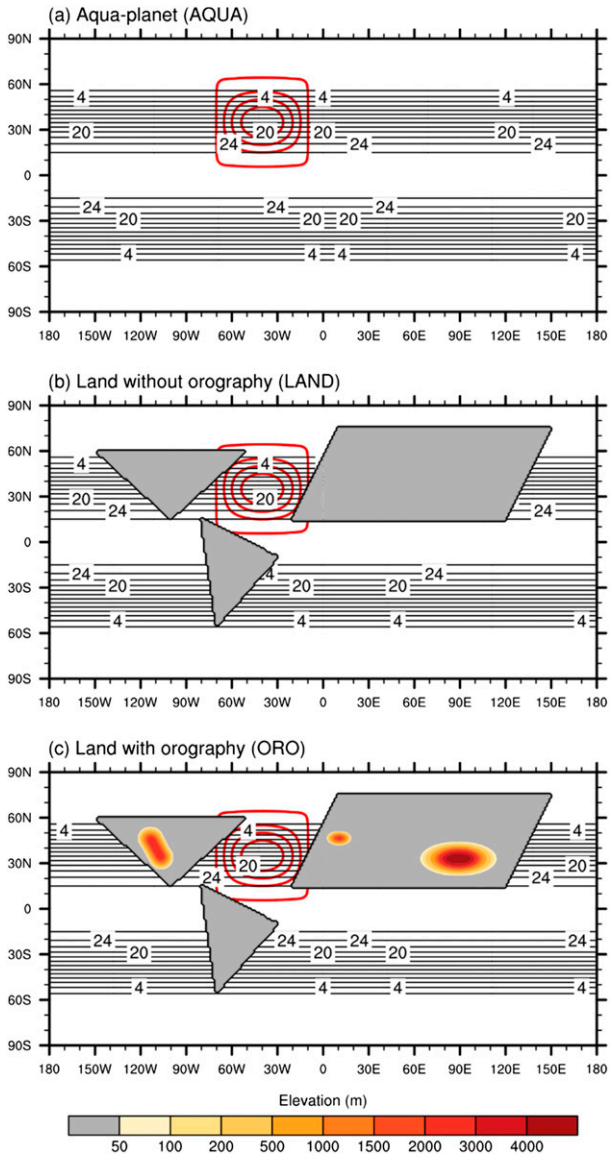

FIG. 1. (a) SST distributions in aquaplanet (AQUA) experiments. (b) Land configuration and SST distributions in land (LAND) experiments. (c) Land and orography and SST distributions in orography (ORO) experiments. Concentric circles in the North Atlantic indicate the location and intensity of the SST anomalies in the warm and cold SST anomaly runs. Outermost contour is 0°C, and the SST anomaly increases or decreases by 1°C intervals, reaching ±4°C at the center. Land elevations are shaded gray in (b) and (c).

The first set of experiments uses an aquaplanet as the lower boundary of the atmosphere (Fig. 1a). In these experiments, and in the later ones, the basic-state and anomalous SST were derived from the Qobs distribution described in Neale and Hoskins (2000) and modified in a manner similar to that in Brayshaw et al. (2008). An advantage of a Qobs-type solution is that it is zonally symmetric. Modifications to the Qobs solution were made to align it better with observed Northern Hemisphere SST during boreal spring. To that end, we used the Second Hadley Centre Sea Surface Temperature dataset (HadSST2; Rayner et al. 2006) for March, from 1961 to 1990, and average the Northern and Southern Hemispheres to obtain an observed SST pattern. We then modified the Qobs solution to best match the observations. After these processes, the global SST is defined as

$$\mathrm{SST}(\phi) = \frac{T_{\max}}{2}\left[2 - \sin^4\left(\frac{18\phi}{13}\right) - \sin^2\left(\frac{18\phi}{13}\right)\right], \qquad (1)$$

where $T_{\max}$ is the maximum temperature (set to be 28°C) and occurs along the equator and ϕ is the latitude. The SST calculated from (1) becomes zero at 62.5° latitude, 2.5° closer to the pole than the SST distribution in Neale and Hoskins (2000). Poleward of 62.5°, SST is set to be 0°C.

For the SST anomaly experiments, we impose a monopole perturbation onto (1). The equation is, after further modifications of that in Brayshaw et al. (2008),

$$\Delta\mathrm{SST}(\phi,\lambda) = \Delta T_{\max}\cos\left[\pi\left(\frac{\lambda-\lambda_0}{\Delta\lambda}\right)\right]\cos^2\left[\left(\frac{\phi-\phi_0}{\Delta\phi}\right)\right]. \qquad (2)$$

In (2), $\Delta T_{\max}$ is the maximum anomaly (±4°C); λ, λ_o, and $\Delta\lambda$ are the longitude, longitude at the anomaly center, and longitudinal radius of the SST anomaly, respectively; and ϕ, ϕ_0, and $\Delta\phi$ are the same as for the SST anomaly but in latitude. The SST anomaly is centered at 32.5°N, 40°W with a 30° radius in both latitude and longitude. It is shown in Fig. 1a by the concentric circles.

It should be noted that we use a maximum SST anomaly magnitude of ±4°C, and it is quite a bit greater than the observed SST anomalies in the AMO (0.5°–1.0°C). Because the only forcing for each set of the model experiments is the SST anomaly, we use such a large SST anomaly to simply increase the signal-to-noise ratio of the responses to the SST anomalies. A similar idea has been used in several previous studies of a similar nature, for example, Brayshaw et al. (2008, who used 3°C for the SST anomaly), Webster (1981, 5°C), and Ting and Held (1990, 2.5° and 5°C). Nonetheless, caution should be observed in interpreting the outcomes of the idealized model runs to focus on the patterns in the response.

We next introduce the simplified geometric dimensions for the continents that will be added to the aquaplanet to represent the North American, South American, and the Eurasian landmasses. The result is shown in Fig. 1b. All three idealized continents have a maximum elevation of 1 m above the sea level to limit any orographic effect on

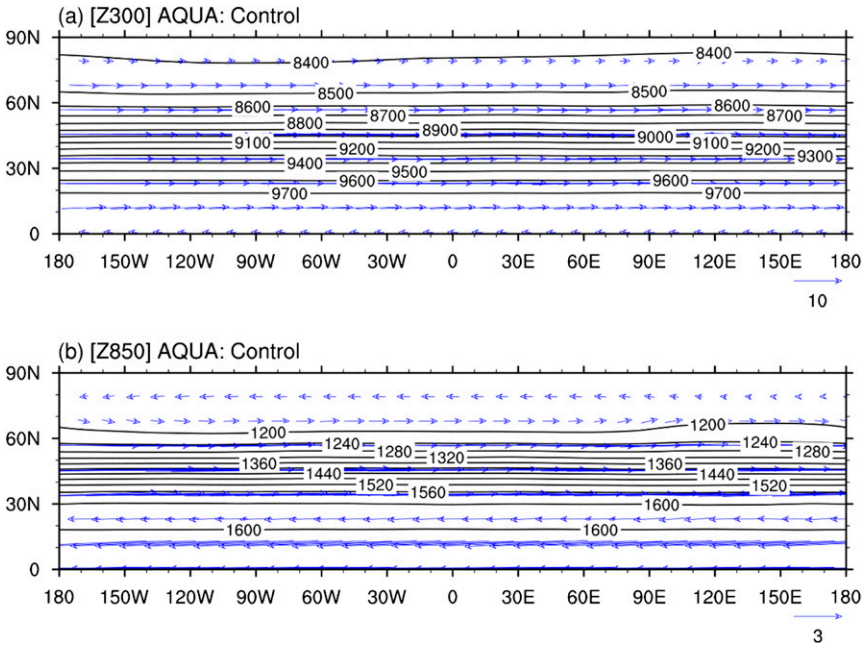

FIG. 2. Equilibrium geopotential heights (contour lines, m) and winds (arrows, m s^{-1}) for the control run at (a) 300 and (b) 850 hPa. Contour interval and reference wind vector are 100 m and 10 m s^{-1}, respectively, in (a), and 40 m, 3 m s^{-1}, respectively, in (b).

the atmosphere. While the land dimensions are idealized, the land surface processes are fully dynamic and described in the land surface model. This allows land surface temperature, soil temperature and moisture, and other surface and soil parameters to change in time. Only a single land surface type, cool grassland, is used across each continent. There are no rivers or coastal irregularities. As a result, there is no surface inhomogeneity that could force small- or regional-scale changes in the atmospheric response over the continents.

In the final set of experiments (Table 1), we add the idealized orography of the Rocky Mountains in North America, and the Alps and the Tibetan Plateau in the Eurasian continent. The shapes are based on Gaussian surfaces and the elevation, aspect ratio, and orientation of these mountains, and are set to be closely representative of their real orographic features (Fig. 1c). Over the elevated land in these mountains and plateau is the same single land surface type (cool grassland) and no rivers and terrain irregularities. Additional details of these model setups are given in Veres (2014).

3. Results and discussions

a. *Atmospheric circulation response to SST anomaly in an aquaplanet*

To examine the atmospheric circulation response to the North Atlantic SST anomaly, it is necessary to provide the background (basic state) circulation that is in equilibrium with the symmetric (control) SST. In the aquaplanet, this basic state of circulation (control run) is shown in Fig. 2 by geopotential height and winds in the lower (850 hPa) and upper (300 hPa) troposphere. Only the circulation in the Northern Hemisphere is shown in Fig. 2. Circulation in the Southern Hemisphere is symmetric over the equinox SST.

In the lower troposphere, Fig. 2b shows fairly uniform low-level easterly trade winds south of the 30°N latitude, and strong westerly winds between 30° and 70°N around the globe. Between these wind regimes is high pressure in the subtropics from 20° to 30°N. The wind regime reverses from westerly to easterly in the high latitude north of 70°N and rotates around the polar high pressure system. In the upper troposphere (Fig. 2a), the wind is primarily westerly, and is the strongest in the subtropical jet and weakest around the polar vortex. These mass and wind regimes are consistent with the zonally symmetric circulation in the equinox, and they describe an idealized unmodified (by land and orography) three-cell circulation that transports heat and energy from the tropics to the poles (e.g., Palmén and Newton 1969, chapters 5 and 6).

After establishing the basic-state circulation with the zonal SST, we add a warm or cold SST anomaly in the North Atlantic latitudes and longitudes in the form described in Eq. (2). The equilibrium solutions from the

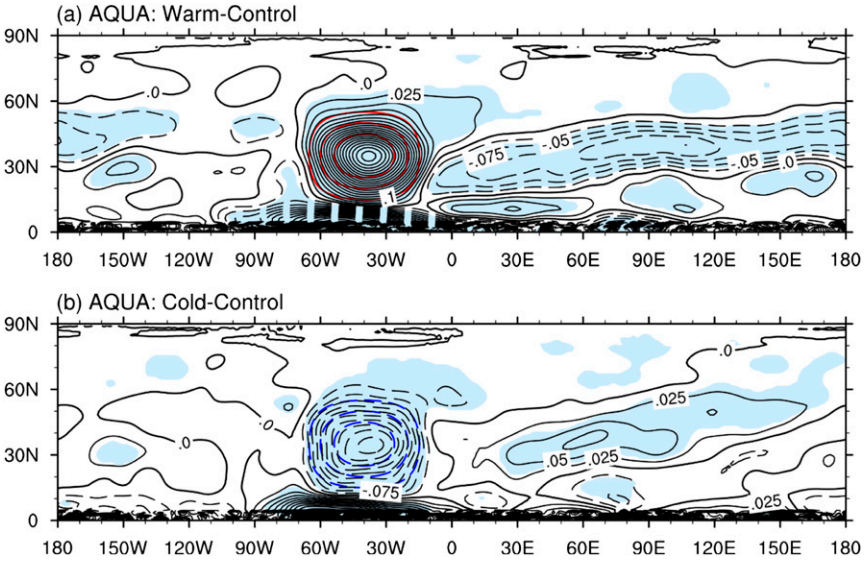

FIG. 3. Anomalies (°C day^{-1}) in diabatic heating (sensible plus latent heating) for (a) warm and (b) cold SST anomalies in the aquaplanet. Contour interval is 0.025°C day^{-1}. Data are filtered using a Gaussian filter. In both panels, shaded regions indicate changes are significant at the 95% confidence level. Warm (red, solid) and cold (blue, dashed) SST anomalies are shown in concentric circles. Contour interval for SST anomaly is 1°C with the greatest magnitude at the center.

model runs in these experiments are examined to evaluate the circulation response (precipitation response is discussed separately in Part II) and reveal their differences forced by the opposite SST anomalies. A direct response to the imposed warm or cold SST anomaly in the North Atlantic is the change in atmospheric diabatic heating over the SST anomaly. This heating consists of surface sensible heat and latent heat in the vertical column above the surface. The latter contains the effect of condensation and its associated latent heat release in convection. The difference in the vertically integrated diabatic heating between the warm SST run and the control run is shown in Fig. 3a. Figure 3b shows the diabatic heating anomaly in the cold SST run from the control run. Note that we have applied a 2D Gaussian filter with a standard deviation (σ) of 4.2° to the data, to enhance the large-scale features of interest (the same filter is applied to all anomalies shown in the figures and is discussed in this paper unless otherwise noted).

As anticipated, more intense convection and latent heating occurs over the region of warmer SST, whereas there is much weaker or a lack of diabatic heating in the same region when the SST is cold. In addition, Fig. 3 suggests organized anomalous circulation by the bands of enhanced or suppressed convection and latent heating. For example, driven by the warm SST (Fig. 3a), there is indication of a weak band of heating anomaly emanating from the warm SST anomaly region eastward between 50° and 60°N. South of this band is a band of severely suppressed convection. It spreads from the subtropics and propagates northeastward to complete the latitude circle around 50°N. The center of the suppressed convection is around 90°E longitude. This center and the enhanced convection over the warm SST region along the same latitude suggest a northward-shifted Walker-type circulation in this idealized experiment. Moreover, this band of suppressed convection or enhanced subsidence may have encouraged, by its strong low-level divergence, convection observed on its north and south sides.

In the cold SST case, the diabatic heating anomalies (Fig. 3b) are nearly opposite of those in the warm SST, but with weaker magnitude. The positive anomaly in latent heat downstream of the cold SST region spreads wider in latitude than the negative anomaly band in the warm SST case. While also propagating into the high latitude, it is quickly disorganized when reaching there, failing to complete the latitude circle. As a result, the upstream of the cold SST region shows poorly organized heating anomalies compared to that in the warm SST case.

The 850- and 300-hPa circulation anomalies in equilibrium with these diabatic heating anomalies are shown in Fig. 4. Responding to warm SST, the negative anomaly in geopotential height develops in the lower troposphere over most of the warm SST region (Fig. 4b). From there, the negative anomaly signal emanates northeastward. At the equilibrium, a wavenumber-1 Rossby wave structure establishes in the subtropics, and also mid- and high

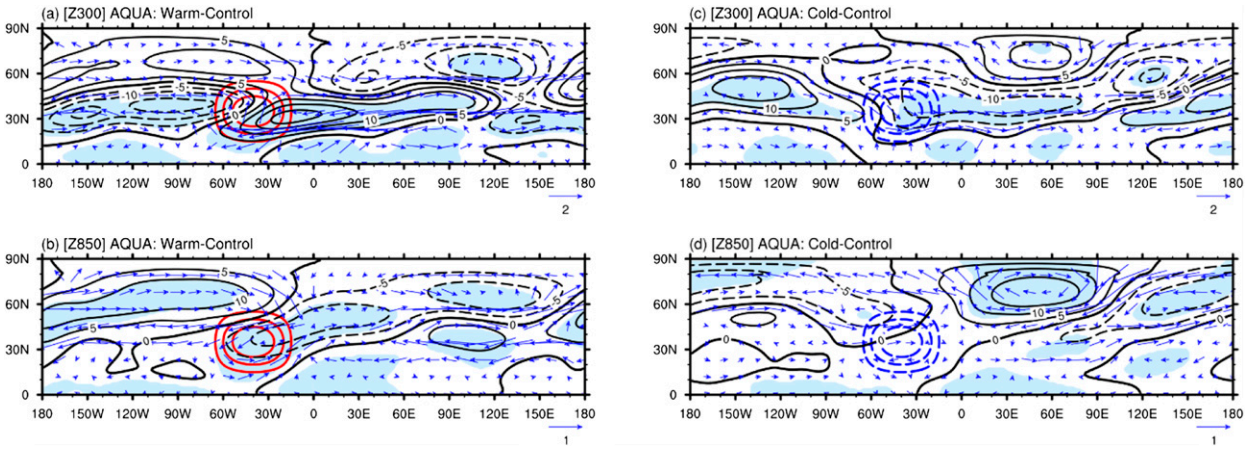

FIG. 4. Anomalies of geopotential height (m, contour lines) and winds (m s^{-1}arrows) at (a),(c) 300 and (b),(d) 850 hPa with the (a),(b) warm and (c),(d) cold SST anomalies in the aquaplanet experiments. Contour intervals are 5 m and reference wind vectors are (a),(c) 2 and (b),(d) 1 m s^{-1}. Data are filtered using a Gaussian filter. Shading indicates changes are significant at the 95% confidence level. Warm (red, solid) and cold (blue, dashed) SST anomalies are shown in concentric circles.

latitude but of nearly a reversed phase. The upper troposphere (Fig. 4a) also shows a strong wavenumber-1 anomaly pattern, but it has positive anomalies east of the warm SST region with a center over the southeastern quadrant of the warm SST region. Upstream of the SST anomaly center are negative anomalies. We also note that this pattern is confined in the latitude width of the SST anomaly from about 15° to 55°N. North of 55°N, geopotential anomalies show a wavenumber-1 pattern but with reversed signs from that in the south. Because of these differences in poleward propagation of responses to the warm SST anomaly between the lower and upper troposphere, the geopotential anomalies in response to the warm SST anomaly have a baroclinic profile south of 55°N, the strongest in the subtropics. Poleward of 55°N, the vertical profile is barotropic.

The tropospheric circulation responses to the cold SST anomaly are quite different from those to the warm SST anomaly. While it may be anticipated that the response to the cold SST anomaly be weaker than that to the warm SST anomaly because of weaker diabatic heating response to the cold SST (Fig. 3), we find it is difficult to draw such a conclusion from observing regions of equally strong responses to the cold as to warm SST anomaly, or even stronger responses to the former than to the latter. This difficulty reflects the effect of the nonlinearity of the circulation in response to the SST forcing. The response to the cold SST anomaly shows little significant response in geopotential at 850 hPa over the cold SST region and along its latitude band around the globe (Fig. 4d). Instead, significant responses are shown in the latitudes poleward of 50°N downstream of the cold SST center, quite different from the response to the warm SST, which is confined between the subtropics and 70°N (Fig. 4b). In the upper troposphere (Fig. 4c), the response is in one wave train confined within the latitude width of the cold SST anomaly. This pattern is similar to that in Fig. 4a but much weaker and with opposite signs.

Although a causal argument for the development of these anomalies shown in the geopotential, as well as other variables, is difficult from these equilibrium—rather than transient—solutions of the model, some physical consistency arguments of the dynamic processes sustaining these equilibrium solutions may still be made. In the following, we highlight the major features in modeled relative vorticity budget to show the vorticity processes that may sustain the equilibrium solutions. Figure 5 shows the mass-divergence-induced local relative vorticity anomaly in the lower and upper troposphere. In the warm SST case at 850 hPa (Fig. 5b), the divergence effect is strongest in the warm SST anomaly region (also in the polar latitude), with a convergence (for positive vorticity) anomaly in the southeastern half of the warm SST and neighboring areas. Over the northern half of the warm SST region is a divergence (for negative vorticity) anomaly. Reversed anomalies in divergence appear in the upper troposphere in those areas (Fig. 5a), consistent with the requirement of mass continuity.

These anomalies in the relative vorticity generation by divergence may explain the geopotential anomaly pattern in equilibrium with the warm SST forcing shown in Figs. 4a and 4b. It is important to note that a direct relation between relative vorticity and geopotential is strictly limited to a quasigeostrophic system (which these simulations are not). However, the quasigeostrophic approximation is generally considered valid in the extratropics,

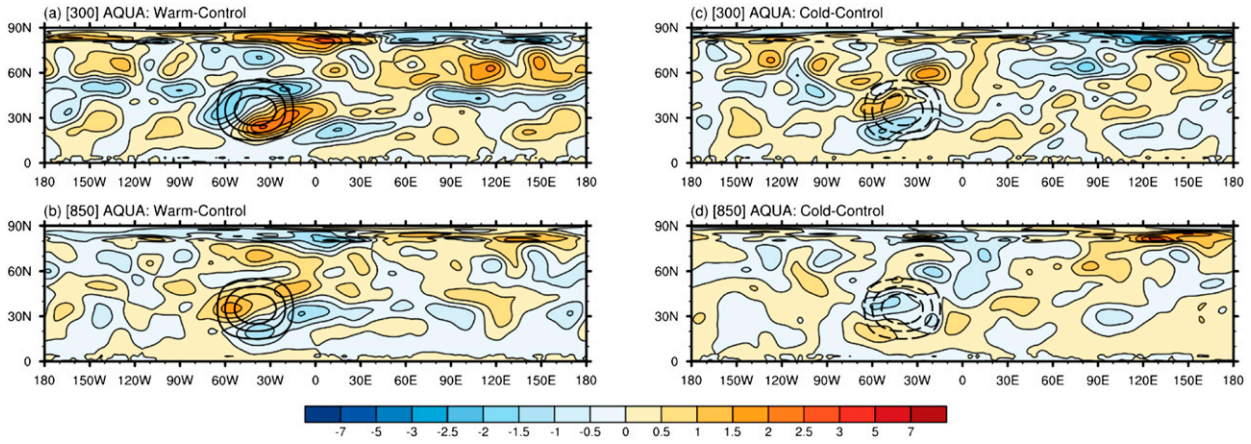

FIG. 5. Anomalies of divergence term in the vorticity equation at (a),(c) 300 and (b),(d) 850 hPa with the (a),(b) warm and (c),(d) cold SST anomalies in the aquaplanet experiments. Units are $1 \times 10^{-7}\,s^{-2}$. Data are filtered using a Gaussian filter. Warm (solid) and cold (dashed) SST anomalies are shown in concentric circles.

and our test calculations of streamfunction and geopotential have produced a nearly identical response, except along the tropics, warranting our use of the quasigeostrophic approximation between the relative vorticity and geopotential.

The negative geopotential anomalies in the central and southern areas of the warm SST center in Fig. 4b are consistent with the local convergence anomaly in Fig. 5b, although there are differences in the details between Figs. 5b and 4b in those areas because of other vorticity processes, such as vertical stretching due to convection. The positive geopotential anomaly in the northern area of the warm SST center is consistent with the strong divergence (negative relative vorticity) anomaly in that area.

This particular distribution of divergence-induced relative vorticity anomalies around the warm SST center could be sustained by the anomalous circulation around the warm SST center. In the transient process reaching the equilibrium condition, it could be that the anomalous cyclonic flow around the warm SST center causes mass divergence and a decrease in relative vorticity along the northerly flow on the western side of the warm SST center, particularly in its northwestern side (net loss of mass by departing to the south). Deposit of mass into the easterly mean flow into the southern side of the warm SST center would induce local convergence. The anomalous westerly flow along the southern side of the warm SST center would also induce mass convergence with the mean easterly flow, increasing the local relative vorticity. In the northeastern and northern sides of the warm SST center, the weak mass divergence could be a result of the variation in the mean wind with latitude from the subtropics to the midlatitudes and its interaction with the anomalous cyclonic circulation around the warm SST center.[2]

In the upper troposphere (Fig. 5a), reversed processes of that described above may have maintained the divergence and relative vorticity and contributed to the reversed geopotential anomaly pattern around the SST anomaly center shown in Fig. 4a.

Outside the warm SST center, the anomalies in the divergence are also supporting parts of the geopotential anomalies. At 300 hPa (Fig. 5a), for example, downstream of the warm SST center, divergence anomalies (thus, negative anomalies of relative vorticity) stretch eastward to about 70°E longitude, explaining the positive geopotential anomaly shown in Fig. 4a. Upstream of the warm SST center, the majority of the convergence (positive relative vorticity) anomalies between 30° and 60°N support the negative geopotential anomaly in Fig. 4a. We also note the differences between changes in divergence-induced relative vorticity and the geopotential, for example, in the downstream high latitude area. Some of those differences could be explained by the advection of relative vorticity, which is particularly strong in the upper troposphere. An example of the effect from advection of relative vorticity will be discussed in the land experiment.

In the cold SST anomaly, a nearly reversed pattern but with smaller magnitude is found in the divergence term.

[2] We note that the center of negative geopotential (low pressure) in this case is shifted to the southern and eastern sides of the warm SST center from the case in Hoskins and Karoly (1981). This difference could result from the presence of the mean flow in this study.

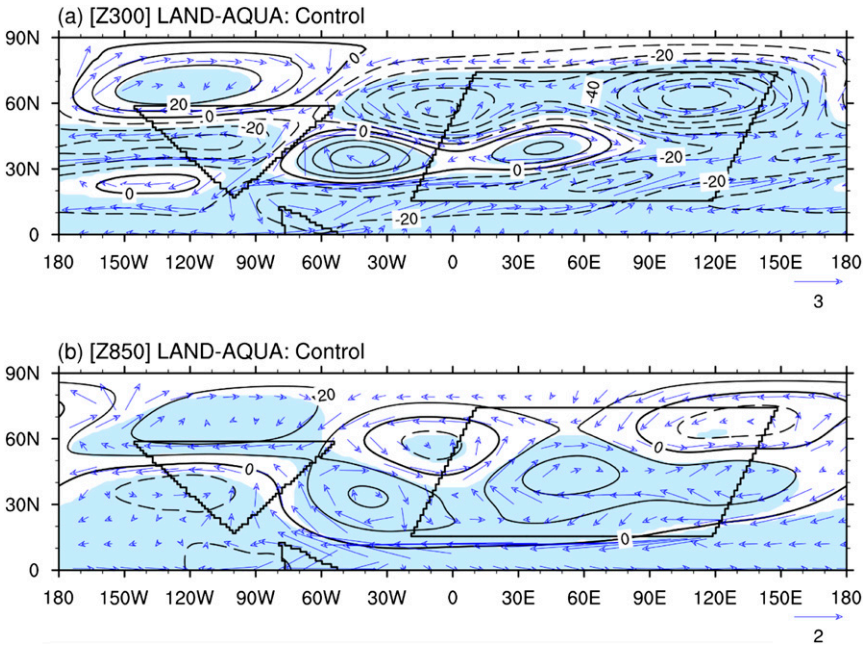

FIG. 6. Differences in geopotential height (m) and winds ($m\,s^{-1}$) between the land and aquaplanet experiments for the control SST at (a) 300 and (b) 850 hPa. Contour interval is 10 m, and the reference wind vectors are (a) 3 and (b) $2\,m\,s^{-1}$. Data are filtered using a Gaussian filter. Shading indicates changes are significant at the 95% confidence level.

At 850 hPa (Fig. 5d), the anomalous anticyclonic circulation around the cold SST center has weak divergence following the northerly flow on the northeastern side of the cold SST center. This flow also generates convergence in the southeastern side of the SST anomaly center, where it converges into the easterly mean flow. On the western side of the cold SST center, the southerly flow causes mass divergence in the southwestern side and convergence in the northwestern side, where the anomalous southerly flow converges into the westerly mean flow. Away from the cold SST center, the relative vorticity anomaly induced by divergence also explains the major feature in the geopotential anomaly shown in Fig. 4d.

At 300 hPa, the anomalous cyclonic circulation over the cold SST center and the divergence-induced vorticity change again, explaining some of the geopotential anomaly pattern. There are large differences between the two, however, in the upstream and in the downstream in high latitudes. They are attributed to the advection of vorticity in those areas.

b. *Circulation response to the SST anomaly in presence of the continents*

The preceding section illustrated the responses of the atmosphere in an aquaplanet to SST anomalies in the North Atlantic. We now introduce the continents (without orography) into the model and examine how the responses to SST anomalies would change.

Figure 6 shows the differences in geopotential height at equilibrium state between the land and the aquaplanet experiment with the climatological SST described in Eq. (1). The first noticeable difference, as anticipated, is the strong zonal asymmetry (wave pattern) in both the lower and upper troposphere, resulting from asymmetrical distributions of the continents. Another important result is that the continents induce anomalies in the circulation that are primarily barotropic. If the surface temperature anomalies are examined (Fig. 7b), we see that the size and shape of each continent affect its temperature and geopotential anomaly distribution.

Figure 7b shows that, compared to the aquaplanet, the massive Eurasian continent causes higher surface temperatures in its southern half (up to +8°C) and much lower temperatures in its northern half (down to −20°C). The surface heating in the southern half induces thermal expansion of the air column in the lower troposphere, decreasing the surface pressure (Fig. 7d) while increasing geopotential at 850 hPa (Fig. 6b). Meanwhile, the intense cooling in the northern half of the continent causes an increase in the surface pressure but a decrease in geopotential aloft. The positive geopotential anomaly in the lower troposphere (850 hPa) in the southern half of the continent strengthens the easterly trade winds along the southern coast of the Eurasian continent.

On the other side, while the smaller and idealized triangular shape of the North American continent has a

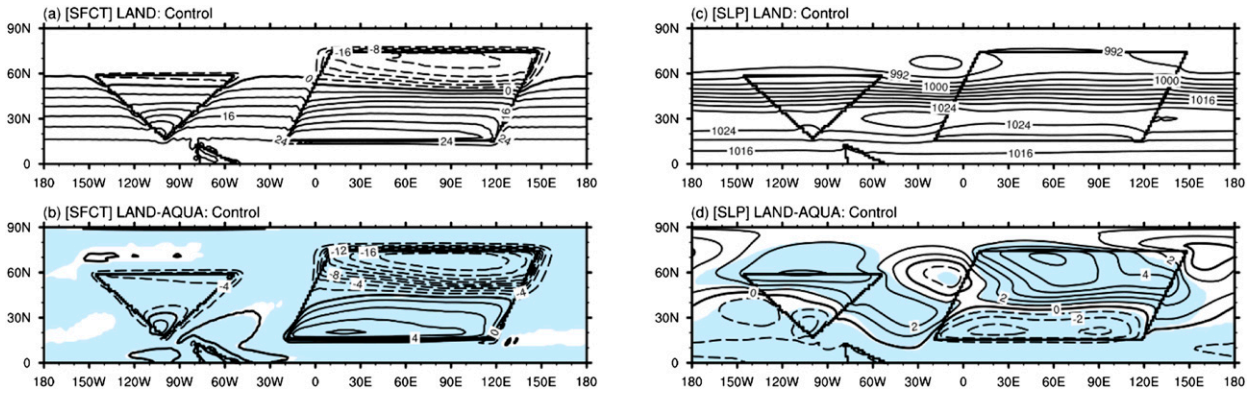

FIG. 7. (a) Surface temperature and (c) sea level pressure (SLP) for the land experiment, and the differences in (b) surface temperature and (d) SLP between the land and aquaplanet experiments for the control SST. Unit for temperature is °C and SLP is hPa. Contour intervals are (a) 4°C, (c) 2°C, (b) 4 hPa, and (d) 1 hPa. Data in (b) and (d) are lightly filtered using a Gaussian filter with $\sigma = 1.4°$. Shading indicates changes are significant at the 95% confidence level.

weaker effect on its surface temperature, it also has cooling in the north (down to about −4°C) and warming in the south (around +2°C) at smaller scales. We can infer from Figs. 6b and 7b that the heating in the south of that continent does not extend far above the surface. As a result, negative geopotential anomalies appear in most of the troposphere (Fig. 6).

The surface warming and associated thermal low near the surface and geopotential anomalies in most of the troposphere (except for 850–700 hPa) over the subtropics of the Eurasian and North American continents create a contrast with relatively cool temperatures and high surface pressure in the same latitudes over the North Atlantic (Figs. 7b and 7d). Such contrast creates a localized high pressure over the subtropical North Atlantic and the formation of the North Atlantic subtropical high pressure system (Fig. 7c and Figs. 6a and 6b). This response to the surface heating over continents is consistent with previous studies on the formation of the subtropical high pressure system (e.g., Liu et al. 2004; Miyasaka and Nakamura 2005), despite the less favorable conditions (equinox) and highly idealized nature of our experiments.

In the high latitudes of the Northern Hemisphere, the relatively warmer ocean off the northern edge of the North American continent and the northward heat transport by the southerly flows diverted by the continent contribute to the positive geopotential anomalies in the lower troposphere (Fig. 6b). However, at the same latitudes in the Eurasian continent, the much colder surface temperature (Fig. 7b) produces high surface pressure (Fig. 7d). Furthermore, the intense surface cooling north of 55°N acts to depress the geopotential in the region, forcing negative geopotential anomalies in the lower troposphere (Fig. 6b). In the upper troposphere (Fig. 6a), we find similar geopotential anomaly patterns over the continents and adjacent oceans, confirming the barotropic profile in response to the lands.

We now examine the effects of the SST anomalies in the North Atlantic Ocean on the circulation in the presence of the continents. Figures 8a and 8b show the geopotential height anomalies at 300 and 850 hPa, respectively, in response to the warm SST anomaly in the land experiment. The pattern of the geopotential anomaly in both the upper and lower troposphere is rather similar to that from the warm SST experiment in the aquaplanet, except for two differences. One of the differences is that the positive or negative anomaly has a wider meridional scale, or that it is less confined in the midlatitude than the response in the aquaplanet. This change must be from the continents, because of the land processes previously discussed. The other difference is that the significant responses are more concentrated downstream of the SST anomaly than those from the aquaplanet run, especially in the upper troposphere.

To explain the more active and enhanced response of geopotential downstream of the warm SST anomaly center, we show again in Figs. 9a and 9b the divergence-induced relative vorticity change in response to the warm SST anomaly in the land experiment. We first notice that the response pattern of the divergence term over the warm SST region is similar to that from the aquaplanet experiment (Figs. 5a and 5b), except that the magnitude is larger. These stronger responses in divergence-induced relative vorticity in the warm SST region result from the land-induced circulation anomalies discussed earlier. We recall that, with the continents there are stronger easterlies in the lower troposphere of the subtropics along the southern tier of the Eurasian continent and weakened westerlies from the midlatitude North American continent

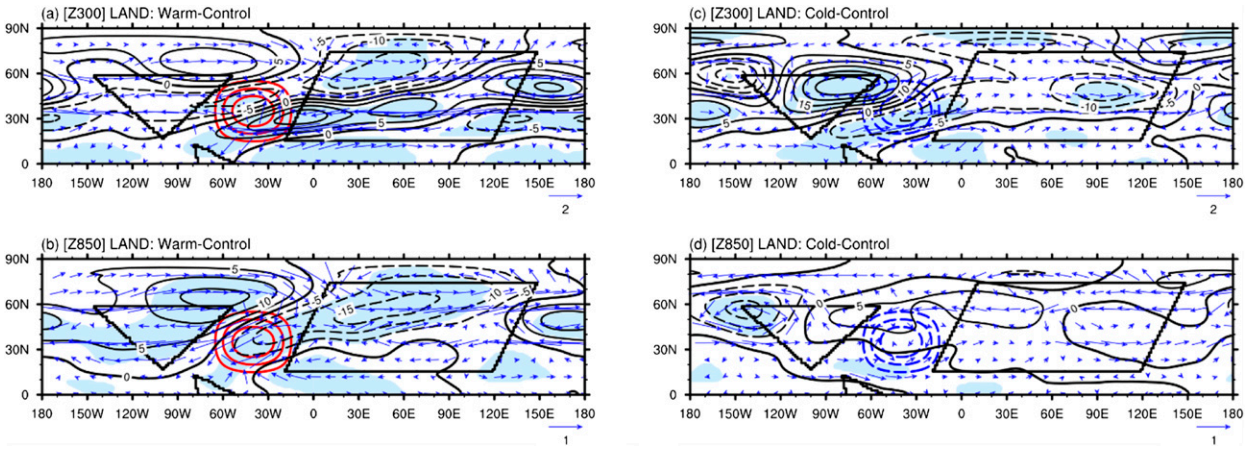

FIG. 8. As in Fig. 4, but for the land experiments.

(Fig. 6b). In the anomalous cyclonic circulation around the warm SST center in the lower troposphere, the continent-enhanced easterlies in the subtropics are going to enhance convergence in the lower troposphere on the southern and southeastern sides of the warm SST center (in processes similar to that discussed for Fig. 5). This enhanced low-level convergence and convection would demand more mass from the northern and northwestern sides of the warm SST center, encouraging stronger divergence in those areas.

The enhanced divergence/relative vorticity response in the lower troposphere also extends over the Eurasian continent, as in the aquaplanet result, but with larger magnitudes, particularly in the central and eastern sections of that continent (Fig. 9b vs Fig. 5b). Meanwhile, upstream in North America, the response has changed little from that in the aquaplanet warm SST experiment. A comparison of this somewhat asymmetric response (to the warm SST center) in the divergence-induced relative vorticity to the response in geopotential in the lower troposphere (Fig. 8b) suggests that the former could be a major source sustaining the latter. However, there are areas where the two do not correspond to each other well, for example, in the western area of the Eurasian continent. Such discrepancies become even larger at 300 hPa. As indicated earlier, they suggest a role of the advection of relative vorticity in the geopotential in response to the SST anomaly, particularly in the upper troposphere. An example is used here to illustrate this role.

The responses of advection of relative vorticity to the warm SST anomaly are shown in Figs. 10a and 10b for the land experiment. In the lower troposphere (Fig. 10b), the response is small (so is its effect on the vorticity), yet a careful examination indicates that its spatial distribution helps compensate/modify the response in vorticity change from divergence (Fig. 9b). These vorticity responses provide a fairly consistent explanation of the geopotential response to the warm SST anomaly (Fig. 8b). In the upper troposphere, the vorticity advection plays a strong role in sustaining the responses of geopotential to the warm SST. Comparing Figs. 9a and 10a, we find that the latter shows quite stronger responses downstream over the Eurasian continent than in North America. In particular, a chain of negative relative vorticity due to the advection effect propagating from the warm SST center to the northeastern corner of the Eurasian continent collocates with the region of strong positive geopotential anomaly shown in Fig. 8a. The stronger response downstream of the warm SST center than the upstream response also is consistent with the slight asymmetry in the response of geopotential at 300 hPa. On both the northern and southern sides of that band, the responses from vorticity advection and convergence-induced vorticity change are consistent with most of the anomalies in geopotential shown in Fig. 8a.[3]

In contrast to these largely similar geopotential responses to the warm SST anomaly in the land and aquaplanet experiments, the geopotential response to the cold SST anomaly in the land experiment is very different from the results from the aquaplanet experiment. These differences are clearly shown by contrasting the results between Figs. 8c and 4c and Figs. 8d and 4d. They can be summarized by a strong asymmetry in the geopotential response, relative to the cold SST center, in the land experiment. In Fig. 8c, active and

[3] We note that the vorticity advection term is very noisy with many local extremes. Their effects are not reflected in the geopotential anomaly, except for the more organized and large-scale anomalies, such as the one discuss in Fig. 10a, because most of them are smoothed out in the much less noisy geopotential field.

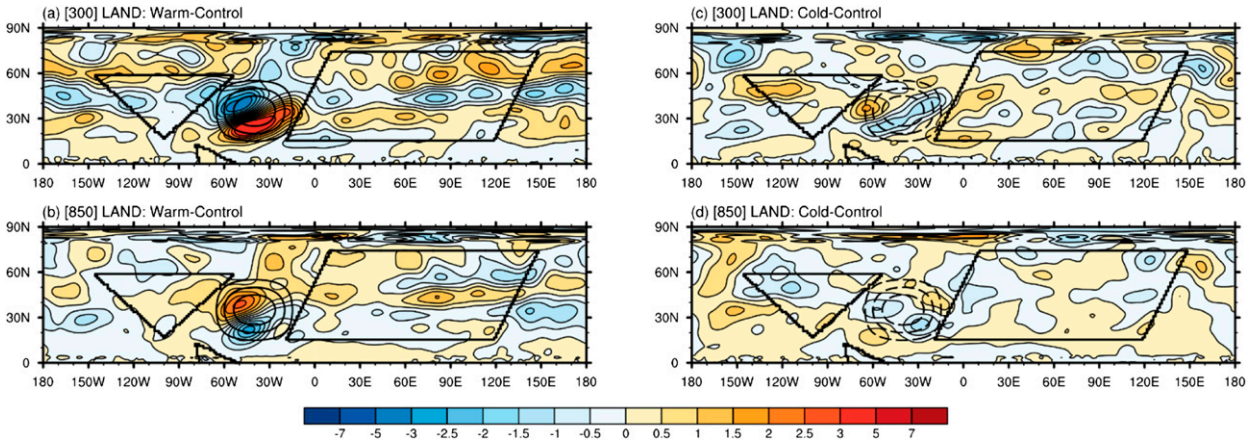

FIG. 9. As in Fig. 5, but for the land experiments.

significant responses are found in the SST anomaly center and upstream. In Fig. 8d, the only one significant response region is shown upstream of the cold SST center. The asymmetric pattern in geopotential response in Fig. 8c is supported by (consistent with) a similar response in advection of relative vorticity to the cold SST anomaly. As shown in Fig. 10c, there are much more intense activities in relative vorticity due to advection over North America than in Eurasia (we further notice that the response in North America in Figs. 8c and 8d is opposite of that in the aquaplanet). While the response in vorticity advection in the lower troposphere (Fig. 10d) also suggests weak asymmetry, the geopotential response pattern in Fig. 8d is seeing more contribution from the vorticity change caused by the divergence term, shown in Fig. 9d. Collective contributions from these vorticity processes in response to the cold SST anomaly sustain the geopotential response in the lower and upper troposphere to the cold SST anomaly.

c. *Circulation response to the SST anomaly in presence of continents and orography*

We now examine the atmospheric response to the SST anomaly in the midlatitude North Atlantic in the presence of the idealized continents with major orography in the Northern Hemisphere, for example, the Rocky Mountains, the Alps, and the Tibetan Plateau. Model runs for these experiments will be referred to as orography experiments.

Figure 11 shows the differences in geopotential height at equilibrium state between the orography and the land experiment with the climatological SST described in Eq. (1). Comparing Figs. 11 and 6, we find a distinctive effect of the orography on atmospheric circulation, that is, strong meridional heat transport to higher latitudes. As a result, there is a systematic increase (decrease) in geopotential/mass north (south) of 35°N latitude, which is the latitude crossing near the center of the Rockies

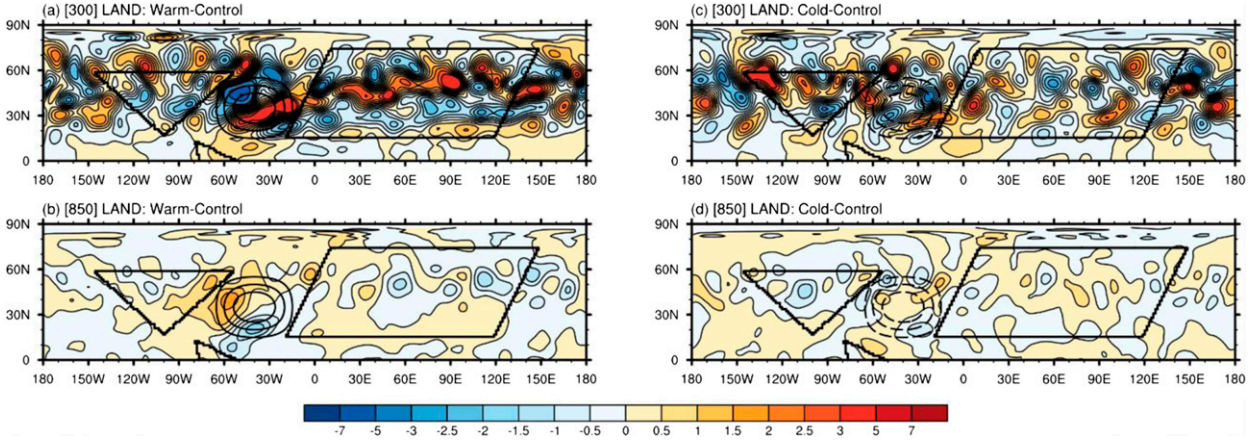

FIG. 10. As in Fig. 9, but for vorticity change caused by advection of relative vorticity.

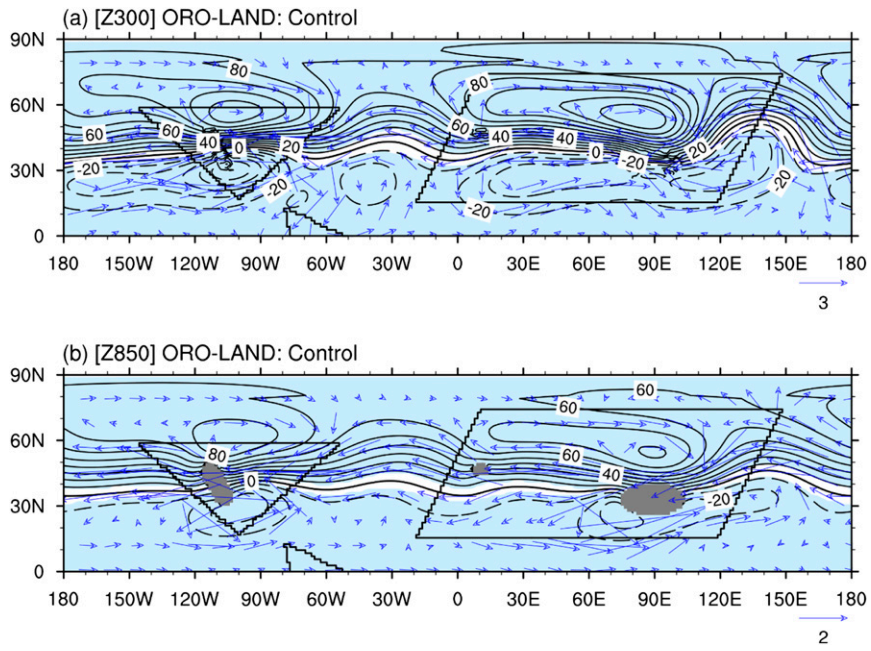

FIG. 11. As in Fig. 6, but for differences between the orography and land experiments.

and the Tibetan Plateau. Note that the scale of the Alps is apparently inadequate to significantly contribute to this transport. Such systematic changes are in strong contrast to the responses of the wavelike pattern in the land experiment (Fig. 6). These changes are taking place through the troposphere, indicated by the barotropic profile. It is also important to indicate that the enhanced poleward transport of mass and heat in the orography world reduces the meridional pressure gradient and therefore the westerlies across the midlatitude.

In the lower troposphere (Fig. 11b), south of 35°N, there are two centers of negative geopotential anomaly attached to the southern edge of the Rocky Mountains and the Tibetan Plateau. Similar anomaly centers are also shown in Ringler and Cook (1999) and Brayshaw et al. (2009), and are interpreted to rise from cyclonic circulation anomalies equatorward of the orographic features. In Brayshaw et al. (2009), the cyclonic anomaly develops from advection of the higher absolute vorticity from the north to the south. Required by the conservation of absolute vorticity, the air column moving southward will increase its relative vorticity to compensate for the decrease in its planetary vorticity. The increase in relative vorticity causes deepening. These stationary cyclonic eddies, somewhat anchored in the south end of the mountains and the plateau, help further divide the subtropical high pressure belt into the North Pacific and the North Atlantic high pressure systems.

With these distinctive features in atmospheric circulation, we now examine the effects of the SST anomalies in the North Atlantic Ocean on the circulation in the orography experiments. Figures 12a and 12b show the geopotential responses to the warm SST anomaly. They show no weak asymmetry as in the response to the warm SST anomaly from the land experiment (Figs. 8a and 8b), yet they resume most of the features from the response to the same SST anomaly from the aquaplanet experiment (Figs. 4a and 4b). Comparing these three sets of responses to the warm SST anomaly in the North Atlantic from the three experiments, we find that in the lower troposphere the response from these different experiments has a similar positive geopotential anomaly in most of North America and a negative anomaly downstream in most of the western Eurasian continent. At 300 hPa (Fig. 12a), the responses are similar with primarily a negative geopotential anomaly in most of North America and positive in most of the western Eurasia, although the negative response over North America is insignificant in the land experiment and has resulted in the weak asymmetric response in that experiment.

The geopotential responses to the cold SST anomaly in the North Atlantic from the orography experiment are shown in Figs. 12c and 12d. Comparing these responses to that from the land and the aquaplanet experiments with cold SST, we find the geopotential responses upstream in North America change considerably between these experiments. For example, in the upper troposphere (Figs. 12c) the major responses in North America are the positive anomaly south of the 50°N and the negative anomaly north of it. A similar pattern of response is

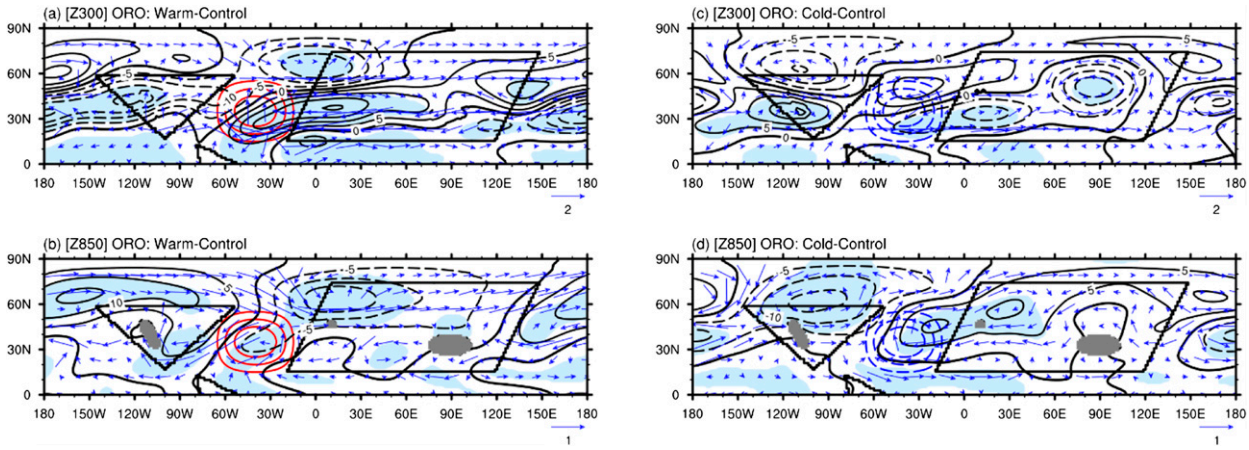

FIG. 12. As in Fig. 4, but for the orography experiments.

shown in the lower troposphere (Fig. 12d), although the negative anomaly in the north spreads farther to the south.[4] This primary meridional gradient in the geopotential anomaly in response to cold SST in the orography experiment is nearly perpendicular to the zonal gradient in the geopotential response to the cold SST in the land experiment (Figs. 8c and 8d). [The geopotential anomaly pattern in Figs. 8c and 8d has a strong positive anomaly in central and eastern North America and a negative anomaly in western and northwestern North America. Further note that this zonal gradient in geopotential response in Figs. 8c and 8d is a reverse of that in Figs. 4c and 4d, showing the response to the cold SST in the aquaplanet experiment.] Downstream of the cold SST center in the Eurasian continent, the geopotential responses between these experiments are different but not as dramatic, however.

The considerable changes in geopotential responses in upstream North America to the cold SST between these experiments, in contrast to changes to the warm SST anomaly, indicate that during the cold SST anomaly the atmospheric circulation is more sensitive, particularly upstream of the cold SST center, to other conditions/forcings—for example, lands and orography—as in these experiments, than during the warm SST anomaly.

The geopotential anomaly pattern in response to the cold SST anomaly in the orography experiment is largely consistent with the responses in divergence-induced and advection of relative vorticity. The former is shown in Figs. 13c and 13d for the upper and lower troposphere, respectively. Although details in changes of this vorticity component do not exactly match that in geopotential anomalies because of other terms and influences, both these figures show more intense divergence-induced vorticity activity in regions from the cold SST anomaly region to upstream North America than in Eurasia. In the lower troposphere (Fig. 13d), from the western side of the cold SST center stretching across the northern half of the North American continent, and further branching into the midlatitude North Pacific, there are mild to strong convergence/positive relative vorticity anomalies. These convergence anomalies match the local negative geopotential anomalies (Fig. 12d). We note that a local dipole in divergence across the Rocky Mountains corresponds to an area of weak negative anomaly in the smoothed geopotential field from North America to the mid–North Pacific in Fig. 12d (see footnote 3). South of this region of negative geopotential anomaly is a region of positive geopotential anomaly, which can be partially sustained by the divergence and resulting negative relative vorticity anomaly in those areas shown in Fig. 13d. A similar analysis of the divergence and advection effects has led to consistent results for the active geopotential responses in the upper troposphere in North America to the cold SST anomaly.

The relatively weak response in geopotential over Eurasia is also consistent, to a large extent, with the divergence-induced relative vorticity response. In Fig. 13d, except for a convergence region in the northwestern area of that continent, there is weak divergence, in the areas of positive geopotential anomaly across the continent. In Fig. 13c, a narrow stretch of the convergence from the southwestern portion to the central portion of the continent is consistent with the negative geopotential anomaly in those areas (Fig. 12c), although the center of the negative geopotential

[4] It is worth mentioning that this anomaly pattern in the troposphere is quite similar to that from a GCM experiment with a fixed cold SST anomaly in the North Atlantic Ocean, described in Hu et al. (2011). As they discussed, this pattern favors a baroclinic environment for development of precipitation in the central U.S. Great Plains.

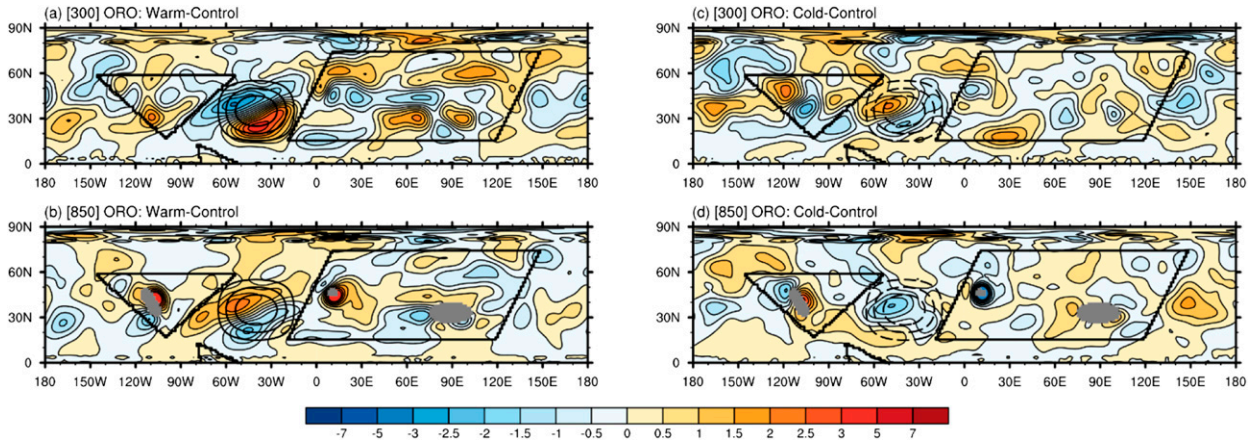

FIG. 13. As in Fig. 9, but for the orography experiments.

in east-central Eurasia is not matched by the weak negative divergence anomaly.

4. Summary and concluding remarks

Using a set of idealized numerical experiments from the NCAR CESM, we have examined the Northern Hemisphere atmospheric responses to SST anomalies in the warm and cold phases of the AMO in the North Atlantic Ocean under equinox conditions. Major findings and their significance are summarized below.

The atmospheric responses to warm SST anomaly are similar among the aquaplanet, land, and orography experiments. In the lower troposphere, they show negative geopotential anomalies emanating to the east of the SST anomaly center (Eurasia) and positive anomalies on the west (North America). Both have poleward phase speed. A reversed geopotential anomaly pattern is shown in the upper troposphere, and the anomalies are confined within the latitudes of the SST anomaly. The responses to the warm SST anomaly have about equal magnitudes over Eurasia and North America.

The geopotential responses to the cold SST anomaly are quite different from responses to the warm SST anomaly. While there is little significant response in the lower troposphere around the cold SST region in the aquaplanet, the response is as strong as in the warm SST case in the land and orography experiments. Outside the cold SST region, the geopotential responses are comparable to the responses to the warm SST anomaly. Organized responses of large amplitude are more concentrated in upstream North America than in Eurasia. Moreover, in North America, the responses change substantially between the experiments. In the orography experiment (closest to the reality), large negative geopotential anomalies appear in northern North America and positive anomalies in the south, showing a meridional gradient in the geopotential in North America in response to the cold SST anomaly. In the land and aquaplanet experiments, the response in North America shows a zonal gradient with opposite signs between each other.

These results show that the atmosphere has distinctive and significant responses to the warm and cold SST anomalies in the midlatitude North Atlantic Ocean. Thus, the observed statistical relationships of the SST variation associated with the AMO and atmospheric circulation and precipitation in North America and Europe (see references in Introduction) are not a statistical coincidence but describe their physical connections. Furthermore, the substantial changes in geopotential response to the cold SST anomaly among the three experiments suggest that the atmosphere may have strong sensitivity to other factors/forcings that may coexist with, or be active in, periods during the cold SST anomaly. This sensitive response of the atmosphere under the cold SST condition, in contrast to the fairly stable or insensitive response to the warm SST in the North Atlantic Ocean, may explain a question we raised earlier, that is, why the warm SST has more consistent response in the atmosphere circulation and precipitation in North America but the response to the cold SST, or anomaly in the cold SST years of the AMO, is rather spotty over the continent. With the warm SST, stable responses are observed, resulting from similar atmospheric processes that contribute to consistent anomalies in circulation and precipitation. However, in the cold SST condition, the sensitive atmospheric response would affect the pattern of the anomalies in time (each year in the cold SST period, the response could be different, to a certain extent, depending on additional forcings) and therefore yield a varying and less persistent pattern in time across North

America. Finally, if this more sensitive response of the circulation to the cold SST anomaly has more of an effect from the weaker diabatic heating response to the cold SST than to the warm SST remains a question.

A ramification of the more sensitive response to the cold SST anomaly than to the warm SST anomaly in the North Atlantic could be an elevated difficulty in making seasonal predictions of precipitation in regions across North America during the cold phase of the AMO. More understanding of this sensitivity is needed to overcome that difficulty and to improve those predictions, as well as interannual to multidecadal time scale predictions of warm-season precipitation in those regions.

Finally, it should be cautioned that the experiments in this study were at equinox conditions and used idealized continents and orography. While these simplifications are necessary to help ubiquitously describe atmospheric responses to the SST anomalies in the North Atlantic (i.e., the intrinsic role of the AMO on atmosphere circulation and precipitation), they pose limitations on the direct application of the results to interpreting the observations. An extension of this work to include transient processes and solutions would be required to overcome such limitations.

Acknowledgments. We thank three anonymous reviewers for their suggestions and comments, which helped improve the clarity of this manuscript. The simulations reported in this work were made using the Yellowstone computing system of the National Center for Atmospheric Research (http://n2t.net/ark:/85065/d7wd3xhc), which is supported by the National Science Foundation. This research was supported by NOAA Grant NA09OAR4310188 and NSF Grant AGS-1103316 to the University of Nebraska–Lincoln and by the USDA Cooperative Research Project NEB-38-088.

REFERENCES

Brayshaw, D. J., B. Hoskins, and M. Blackburn, 2008: The storm-track response to idealized SST perturbations in an aquaplanet GCM. *J. Atmos. Sci.,* **65,** 2842–2860, doi:10.1175/2008JAS2657.1.

——, ——, and ——, 2009: The basic ingredients of the North Atlantic storm track. Part I: Land–sea contrast and orography. *J. Atmos. Sci.,* **66,** 2539–2558, doi:10.1175/2009JAS3078.1.

——, ——, and ——, 2011: The basic ingredients of the North Atlantic storm track. Part II: Sea surface temperatures. *J. Atmos. Sci.,* **68,** 1784–1805, doi:10.1175/2011JAS3674.1.

Enfield, D. B., A. M. Mestas-Nuñez, and P. J. Trimble, 2001: The Atlantic multidecadal oscillation and its relation to rainfall and river flows in the continental U.S. *Geophys. Res. Lett.,* **28,** 2077–2080, doi:10.1029/2000GL012745.

Higgins, R. W., Y. Yao, E. S. Yarosh, J. E. Janowiak, and K. C. Mo, 1997: Influence of the Great Plains low-level jet on summertime precipitation and moisture transport over the central United States. *J. Climate,* **10,** 481–507, doi:10.1175/1520-0442(1997)010<0481:IOTGPL>2.0.CO;2.

Hoskins, B. J., and D. J. Karoly, 1981: The steady linear response of a spherical atmosphere to thermal and orographic forcing. *J. Atmos. Sci.,* **38,** 1179–1196, doi:10.1175/1520-0469(1981)038<1179:TSLROA>2.0.CO;2.

Hu, Q., and S. Feng, 2001a: Climatic role of the southerly flow from the Gulf of Mexico in interannual variations in summer rainfall in the central United States. *J. Climate,* **14,** 3156–3170, doi:10.1175/1520-0442(2001)014<3156:CROTSF>2.0.CO;2.

——, and ——, 2001b: Variations of teleconnection of ENSO and interannual variation in summer rainfall in the central United States. *J. Climate,* **14,** 2469–2480, doi:10.1175/1520-0442(2001)014<2469:VOTOEA>2.0.CO;2.

——, and ——, 2008: Variation of the North American summer monsoon regimes and the Atlantic multidecadal oscillation. *J. Climate,* **21,** 2371–2383, doi:10.1175/2007JCLI2005.1.

——, and ——, 2010: Influence of the Arctic oscillation on central United States summer rainfall. *J. Geophys. Res.,* **115,** D01102, doi:10.1029/2009JD011805.

——, and ——, 2012: AMO- and ENSO-driven summertime circulation and precipitation variations in North America. *J. Climate,* **25,** 6477–6495, doi:10.1175/JCLI-D-11-00520.1.

——, ——, and R. Oglesby, 2011: Variations in North American summer precipitation driven by the Atlantic multidecadal oscillation. *J. Climate,* **24,** 5555–5570, doi:10.1175/2011JCLI4060.1.

Inatsu, M., H. Mukougawa, and S. Xie, 2003: Atmospheric response to zonal variations in midlatitude SSTL transient and stationary eddies and their feedback. *J. Climate,* **16,** 3314–3329, doi:10.1175/1520-0442(2003)016<3314:ARTZVI>2.0.CO;2.

Liu, Y., G. Wu, and R. Ren, 2004: Relationship between the subtropical anticyclone and diabatic heating. *J. Climate,* **17,** 682–698, doi:10.1175/1520-0442(2004)017<0682:RBTSAA>2.0.CO;2.

McCabe, G. J., M. A. Palecki, and J. L. Betancourt, 2004: Pacific and Atlantic Ocean influences on multidecadal drought frequency in the United States. *Proc. Natl. Acad. Sci. USA,* **101,** 4136–4141, doi:10.1073/pnas.0306738101.

Miyasaka, T., and H. Nakamura, 2005: Structure and formation mechanisms of the Northern Hemisphere summertime subtropical highs. *J. Climate,* **18,** 5046–5065, doi:10.1175/JCLI3599.1.

Mo, K., J. Nogues-Paegle, and R. W. Higgins, 1997: Atmospheric process associated with summer floods and droughts in the central United States. *J. Climate,* **10,** 3028–3046, doi:10.1175/1520-0442(1997)010<3028:APAWSF>2.0.CO;2.

Namias, J., 1983: Some causes of United States drought. *J. Climate Appl. Meteor.,* **22,** 30–39, doi:10.1175/1520-0450(1983)022<0030:SCOUSD>2.0.CO;2.

Neale, R. B., and B. J. Hoskins, 2000: A standard test for AGCMs including their physical parameterizations: I: The proposal. *Atmos. Sci. Lett.,* **1,** 101–107, doi:10.1006/asle.2000.0022.

Palmén, E., and C. W. Newton, 1969: *Atmospheric Circulation Systems: Their Structural and Physical Interpretation.* International Geophysics Series, Vol. 13, Academic Press, 602 pp.

Rayner, N. A., P. Brohan, D. E. Parker, C. K. Folland, J. J. Kennedy, M. Vanicek, T. Ansell, and S. F. B. Tett, 2006: Improved analyses of changes and uncertainties in sea surface temperature measured in situ since the mid-nineteenth century: The HadSST2 data set. *J. Climate,* **19,** 446–469, doi:10.1175/JCLI3637.1.

Ringler, T. D., and K. H. Cook, 1999: Understanding the seasonality of orographically forced stationary waves: Interaction between mechanical and thermal forcing. *J. Atmos. Sci.,* **56,** 1154–1174, doi:10.1175/1520-0469(1999)056<1154:UTSOOF>2.0.CO;2.

Schubert, S. D., M. J. Suarez, P. J. Pegion, R. D. Koster, and J. T. Bachmeister, 2004: Causes of long-term drought in the U.S. Great Plains. *J. Climate,* **17,** 485–503, doi:10.1175/1520-0442(2004)017<0485:COLDIT>2.0.CO;2.

Ting, M., 1994: Maintenance of northern summer stationary waves in a GCM. *J. Atmos. Sci.,* **51,** 3286–3308, doi:10.1175/1520-0469(1994)051<3286:MONSSW>2.0.CO;2.

——, and I. M. Held, 1990: The stationary wave response to a tropical SST anomaly in an idealized GCM. *J. Atmos. Sci.,* **47,** 2546–2566, doi:10.1175/1520-0469(1990)047<2546:TSWRTA>2.0.CO;2.

——, and H. Wang, 1997: Summertime U.S. precipitation variability and its relation to Pacific sea surface temperature. *J. Climate,* **10,** 1853–1873, doi:10.1175/1520-0442(1997)010<1853:SUSPVA>2.0.CO;2.

Veres, M. C., 2014: Springtime atmospheric responses to North Atlantic SST anomalies in idealized GCM experiments: Northern Hemisphere circulation and North American precipitation. Ph.D. dissertation, University of Nebraska–Lincoln, 125 pp.

——, and Q. Hu, 2013: AMO-forced regional processes affecting summertime precipitation variations in the central United States. *J. Climate,* **26,** 276–290, doi:10.1175/JCLI-D-11-00670.1.

Wang, C., C. Lee, and D. B. Enfield, 2008: Climate response to anomalously large and small Atlantic warm pools during the summer. *J. Climate,* **21,** 2437–2450, doi:10.1175/2007JCLI2029.1.

Wang, S., and T. Chen, 2009: The late-spring maximum of rainfall over the U.S. central plains and the role of the low-level jet. *J. Climate,* **22,** 4696–4709, doi:10.1175/2009JCLI2719.1.

Webster, P. J., 1981: Mechanisms determining the atmospheric response to sea surface temperature anomalies. *J. Atmos. Sci.,* **38,** 554–571, doi:10.1175/1520-0469(1981)038<0554:MDTART>2.0.CO;2.